Surface vibrational modes of the topological insulator Bi_2Se_3 observed by Raman spectroscopy

H.-H. Kung,[1,*] M. Salehi,[1,2] I. Boulares,[3] A. F. Kemper,[4] N. Koirala,[1] M. Brahlek,[1] P. Lošťák,[5] C. Uher,[3] R. Merlin,[3] X. Wang,[1,6] S.-W. Cheong,[1,6] S. Oh,[1] and G. Blumberg[1,7,†]

[1]*Department of Physics & Astronomy, Rutgers University, Piscataway, NJ 08854, USA*
[2]*Department of Materials Science and Engineering, Rutgers University, Piscataway, NJ 08854, USA*
[3]*Department of Physics, University of Michigan, Ann Arbor, Michigan 48109-1040, USA*
[4]*Department of Physics, North Carolina State University, Raleigh, North Carolina 27695, USA*
[5]*Faculty of Chemical Technology, University of Pardubice, Studentska 573, 53210 Pardubice, Czech Republic*
[6]*Rutgers Center for Emergent Materials, Rutgers University, Piscataway, NJ 08854, USA*
[7]*National Institute of Chemical Physics and Biophysics, 12618 Tallinn, Estonia*

(Dated: November 17, 2016)

We present polarization resolved Raman scattering study of surface vibration modes in the topological insulator Bi_2Se_3 single crystal and thin films. Besides the 4 Raman active bulk phonons, we observed 4 additional modes with much weaker intensity and slightly lower energy than the bulk counterparts. By symmetry analysis and comparison with theoretical calculation, we assigned these additional modes to out-of-plane surface phonons, where the frequency is slightly modified from the bulk phonon due to out-of-plane lattice distortion near the crystal surface. In particular, two of the surface modes at 60 and 173 cm^{-1} are associated with Raman active A_{1g} bulk phonon modes, the other two at 136 and 158 cm^{-1} are associated with infrared active bulk phonons with A_{2u} symmetry. The latter become Raman allowed due to restriction of crystalline symmetry from D_{3d} in the bulk to C_{3v} at the surface of Bi_2Se_3. The 158 cm^{-1} surface phonon mode show a Fano line shape, suggesting interaction with an electronic continuum at the crystal surface. In addition, we observed two weak features at 67 and 126 cm^{-1} likely corresponding to in-plane surface vibrational modes.

I. INTRODUCTION

Topological insulators (TIs) are a new class of quantum matter characterized by linearly dispersed spin polarized gapless surface states within the bulk band gaps [1–8], which may lead to realization of novel phenomena and applications such as spintronics and quantum computing [8–17].

Despite the topological protection, the surface states away from the Dirac point suffer from hexagonal warping effect, resulting in increased scattering rate at the TI surface [18–20]. Among many possible scattering mechanisms, electron-phonon interaction is especially important due to its direct impact on device applications at finite temperature [21]. In particular, the energies and symmetries of the surface vibrational modes are important for modeling the possible relaxation channels of the surface state excitations.

Theoretical modeling of surface lattice dynamics was first developed by Lifshitz and Rosenzweig [22, 23], and later expended by various workers [24–27]. The basic idea is to consider the free surface as a perturbation of an infinite lattice, and therefore to derive the surface modes from the spectrum of bulk vibrations. However, it is often experimentally challenging to distinguish surface signal from the overwhelmingly stronger intensity contribution of the bulk.

Bi_2Se_3 is one of the most studied TI due to its relatively simply band structure, i.e., a single Dirac cone within the 0.3 eV bulk band gap, much larger than the thermal energy at the room temperature. Several papers have studied the surface vibration modes in Bi_2Se_3. Zhu and coworkers observed strong Kohn anomaly at about $2k_F$ using helium atom scattering (HAS) [28], and deduced the interaction between surface phonon and the Dirac electrons to be much stronger than the values previously reported by angle-resolved photoemission spectroscopy (ARPES) measurements [19, 29–31], suggesting that the electron-phonon coupling on TI surface may be more complicated than anticipated. Time-resolved ARPES study on single crystals reported the observation of one A_{1g} bulk phonon at about 74 cm^{-1}, and an additional mode with slightly lower energy, which was interpreted as a surface phonon associated with the observed A_{1g} bulk phonon. However, alternative results have also been reported [31–34], suggesting the existence of multiple phononic decaying channels which may even depend on details of sample preparation. Electron energy loss spectroscopy (EELS) study has distinguish a weak mode at about 160 cm^{-1} in Bi_2Se_3, which was assigned to the surface vibration mode associated with an A_{1g} bulk phonon [35]. The Raman scattering work on bulk single crystal [36] and exfoliated nano-crystals reported several additional features, and were attributed to infrared active phonon modes becoming Raman active due to inversion

* skung@physics.rutgers.edu
† girsh@physics.rutgers.edu

TABLE I. Samples measured in this study.

Sample #	Composition	Description	Growth
#2	Bi_2Se_3	50 QL thin film	MBE
#8	$(Bi_2Se_3)_m(In_2Se_3)_n$	50 nm superlattice with (m,n)=(5,5)	MBE
#10	$(Bi_2Se_3)_m(In_2Se_3)_n$	50 nm superlattice with (m,n)=(10,5)	MBE
#13	$Bi_{1.95}In_{0.05}Se_3$	single crystal with indium doping	Bridgman
#14	Bi_2Se_3	pristine single crystal	Bridgman
#A	Bi_2Se_3	pristine single crystal	Bridgman

symmetry breaking at crystal surface [37, 38].

To date, different surface modes were measured by several distinct techniques, with slight discrepancies between the results and interpretations. Such discrepancy have caused confusion. It is therefore desirable to observe all surface vibration modes within one technique that provides both high energy resolution and symmetry information.

Here, we use high resolution polarization resolved Raman spectroscopy to measure the vibrational modes of both bulk and thin film Bi_2Se_3 samples. In addition to the 4 Raman active bulk phonons, we observed 6 additional modes with about 20 times weaker intensities compared to the bulk phonons (Fig. 1). Raman spectroscopy is a conventional tool for studying phonon modes, and has been used to study the surface lattice dynamics in semiconductors for many years [39]. By comparing to the results obtained by other techniques and calculations, we assigned the observed additional features to surface vibrational modes associated with the bulk phonons due to out-of-plane lattice distortion near crystal surface.

This paper is organized as follows. In Sec. II, we introduce the experiments including sample preparations and the Raman probe. In Sec. III, we present the low temperature polarized Raman spectra of bulk and thin film Bi_2Se_3 samples. Sec. IV discusses the symmetries and microscopic views of the surface vibration modes. Finally, we conclude our discussions in Sec. V.

II. EXPERIMENTAL SETUP

The list of Bi_2Se_3 samples measured in this study is given in Table I. The bulk single crystals were grown by modified Bridgman method. The thin film samples were epitaxially grown on Al_2O_3 (0001) substrates in a custom designed molecular beam epitaxy (MBE) chamber [40, 41]. They were immediately transfered into a cryostat after taking out of MBE chamber.

The superlattice thin films of $(Bi_2Se_3)_m(In_2Se_3)_n$ are grown along (0001) surface [40], where each primitive cell consists of m QL Bi_2Se_3 and n QL In_2Se_3, with each QL being ~ 1 nm thick. Notice that the light penetration depth in In_2Se_3 within energy range of current study is about 100 nm [42], which is about 10 times larger than the penetration depth in Bi_2Se_3 [43]. Therefore, the scattering volume in the superlattice samples is practically the same as bulk.

Bi_2Se_3 has a rhombohedral crystal structure with the D_{3d} point group symmetry. The irreducible representations and Raman selection rules are given in Table II. With 5 atoms in a primitive unit cell, there are a total of 3 acoustic and 12 optical bulk phonon branches. At the Γ-point, the irreducible representations of the Raman active phonons are $2A_{1g} + 2E_g$, and the infrared active phonons are $2A_{2u} + 2E_u$ [44, 45]. These bulk phonon modes have been measured by Raman and infrared spectroscopy [36, 44–47], and the values reported in Ref. 36 and Ref. 47 are listed in Table III.

The crystal naturally cleaves along the (111) surface terminated at Se atoms, forming optically flat quintuple layers (QLs) weakly bonded by van der Waals force [44]. The surface QL has the symmorphic $P6mm$ wallpaper group symmetry (two dimensional crystallographic point group C_{6v}) [48–50]. Since the surface layer phonon modes in Bi_2Se_3 are not perfectly localized and decay into the bulk, it is more appropriate to analyze our experimental results within the layer group $P3m1$ (crystallographic point group C_{3v}, which is a subgroup containing common symmetry operators of D_{3d} and C_{6v} groups) [49].

All Raman scattering measurements are taken from ab surfaces freshly cleaved or grown prior to measurements. Sample #2–14 are measured in a quasi-backscattering geometry in a continuous He-flow optical cryostat. We use λ_L =532 nm solid state laser for excitation, where the spot size is roughly 50 μm. The scattered light was analyzed and collected by a custom triple-grating spectrometer equipped with a liquid nitrogen cooled CCD detector. As for the data collected from sample #A, measurements were done in a back-scattering geometry from a cold-finger cryostat. An Argon ion laser and a home built Ti:Sapphire laser were used as sources, where the spot sizes are roughly 35 and 55 μm, respectively. The scattered light was collected using a triple stage spectrometer (Dilor XY) and imaged on a CCD camera.

All spectra shown were corrected for the spectral response of the spectrometer and CCD to obtain the Raman intensity $I_{\mu\nu}(\omega, T)$, which is related to the Raman response function $\chi''_{\mu\nu}(\omega, T)$ by the Bose factor $n(\omega, T)$: $I_{\mu\nu}(\omega, T) = [1 + n(\omega, T)]\chi''_{\mu\nu}(\omega, T)$. Here, μ

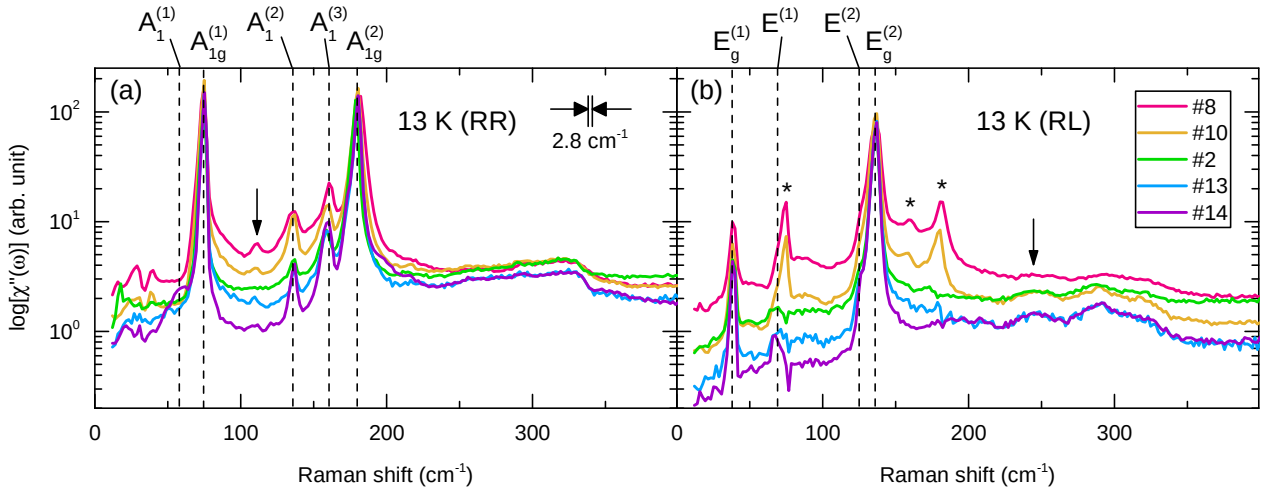

FIG. 1. (Color online) The Raman response function $\chi''(\omega)$ measured in the (a) RR and (b) RL scattering geometry at 13 K from various Bi_2Se_3 samples as described in Table I, plot in semi-log scale. The dashed lines label the observed phonon modes as tabulated in Table III. (a) The mode at 110 cm^{-1} indicated by arrow is due to the phonon signal from α-In_2Se_3 layers [51]. The asterisks mark the phonon modes with A_{1g} and A_1 symmetries, appear in RL geometry due to indium atom diffusion. The instrumental resolution of 2.8 cm^{-1} is shown.

(ν) denotes the polarization of incident (scattered) photon, ω is energy and T is temperature. The scattering geometries used in this experiment are denoted as $\mu\nu = RR, RL, XX$ and YX, which is short for $\overline{z}(\mu\nu)z$ in Porto's notation. R = X+iY and L = X−iY denotes the right- and left-circular polarizations, respectively, where X (Y) denotes linear polarization parallel (perpendicular) to the plane of incidence. The irreducible representations of the D_{3d} and C_{3v} groups corresponding to these scattering geometries are listed in Table II.

Notice that in both the D_{3d} and C_{3v} groups, the phonon intensities do not depend on the orientation of the crystallographic axis. The notations X and Y have no reference to the crystallographic a and b axes. The degree of polarization leakage from optical elements are determined from the $A_{1g}^{(1)}$ and $A_{1g}^{(2)}$ bulk phonons of single crystal samples at room temperature, and was used to remove polarization leakage in all presented data.

TABLE II. The Raman selection rules in the bulk and on the surface of Bi_2Se_3. Notice that upon the restriction of symmetry from point group D_{3d} to C_{3v}, the A_{1g} and A_{2u} irreducible representations merge into A_1, A_{2g} and A_{1u} merge into A_2, E_g and E_u merge into E. [52]

Scattering geometry	Bulk (D_{3d})	Surface (C_{3v})
RR	$A_{1g} + A_{2g}$	$A_1 + A_2$
RL	$2E_g$	$2E$
XX	$A_{1g} + E_g$	$A_1 + E$
YX	$A_{2g} + E_g$	$A_2 + E$

III. RESULTS

Figure 1 shows the Raman response function $\chi''(\omega)$, taken at 13 K with 532 nm excitation, plot in semi-log scale. In order to confirm the tiny features of surface modes, we compared the results from bulk crystals and MBE thin films. Fig. 1(a) and 1(b) are measured with the RR and RL scattering geometries, respectively (Table II). The dashed lines label the observed phonons as tabulated in Table III. The strong modes at 72 and 174 cm^{-1} in RR scattering geometry are the bulk A_{1g} phonons of Bi_2Se_3 (Fig. 1(a)), and the strong modes centered at 37 and 132 cm^{-1} in RL are the bulk E_g phonons (Fig. 1(b)), consistent with previous Raman studies [36, 46] and calculations [53].

The broad feature at about 330 cm^{-1} in RR is possibly due to second-order scattering of the $A_{1g}^{(2)}$ phonon, broadened due to the large downward dispersion of the phonon branch [53]. Similarly, the broad feature observed around 300 cm^{-1} in RL is assigned to two-phonon excitation, $A_{1g}^{(2)} + E_g^{(2)}$. The broad feature at about 245 cm^{-1} (Fig. 1(b), marked by arrow) was previously assigned to the 2D stretching mode of Se atoms on the surface [54]. However, we do not observe the reported resonance effect of this mode with near-infrared excitation (Fig. 2). Notice that this mode energy is also consistent with the two-phonon excitation of $A_{1g}^{(2)} + E_g^{(1)}$.

In order to distinguish the broad features from electronic origin, such as excitations from the topological surface states, we compared the results with indium doped Bi_2Se_3 in Fig. 1. Indium doping was shown to increase the carrier density and suppress the topological surface states in Bi_2Se_3 [40, 55]. Here, we collected data from

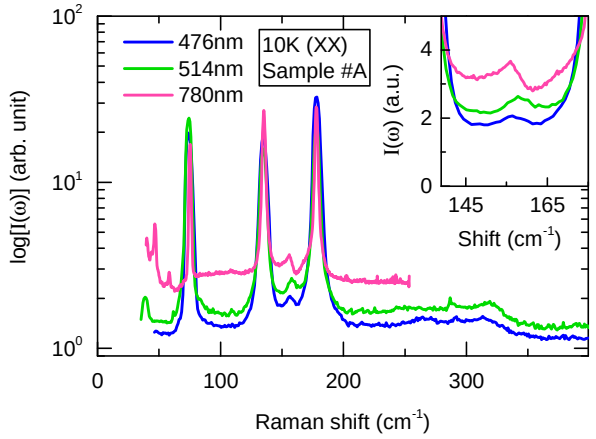

FIG. 2. (Color online) The signal intensity in the XX scattering geometry, measured at 10 K from a bulk Bi_2Se_3 single crystal, plot in semi-log scale. The blue, green and pink lines corresponds to laser excitation energy of 476, 514 and 780 nm, respectively. Inset: enlarged plot around the $A_1^{(3)}$ mode.

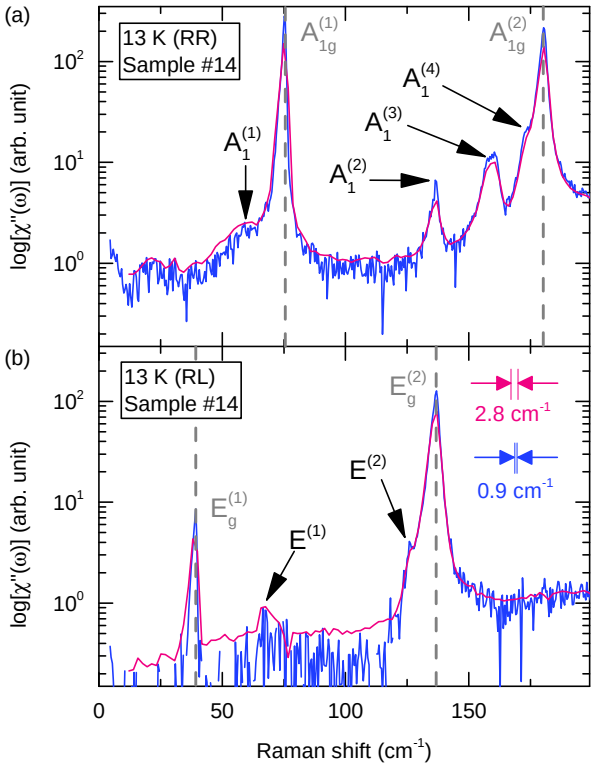

FIG. 3. (Color online) The Raman spectra taken with the (a) RR and (b) RL scattering geometry at 13 K from a bulk Bi_2Se_3 single crystal are plotted in semi-log scale. The red and blue curves correspond to instrumental resolution of 2.8 and 0.9 cm^{-1} (as shown in (b)), respectively. The bulk phonons are marked by gray dashed lines.

bulk single crystals and MBE grown In_2Se_3/Bi_2Se_3 superlattices, where indium doping is achieved through diffusion in the superlattices [56]. In all indium doped samples, the broad features show the same intensity, suggesting their origin unrelated to the topological surface states. This feature is slightly weaker in the superlattice sample #8, despite the first-order phonon modes are still sharp and strong. However, this is likely mainly due to the indium atom diffusion into the Bi_2Se_3 layer breaks the translation symmetry, and therefore further broadens the multi-phonon mode. The indium atom diffusion is also supported by the non-negligible intensity of A_{1g} and A_1 symmetry modes present in RL for both superlattice samples (Fig. 1(b), marked by asterisks). The diffused indium atoms lower the local crystal symmetry in the Bi_2Se_3 layers, and therefore allows vibration modes with A_{1g} and A_1 symmetries to appear in the RL geometry, which is otherwise forbidden for the crystal symmetry of Bi_2Se_3. The small feature at 110 cm^{-1} in RR is due to a strong phonon of α-In_2Se_3 layers [51] (indicated by arrow in Fig. 1(a)).

In addition to the strong bulk first-order Raman phonons and the broad features, we see some additional sharp modes that are about 20 times weaker than the bulk phonons. In Fig. 1(a), two additional sharp features at 136 and 158 cm^{-1} are seen in all samples in RR scattering geometry, labeled $A_1^{(2)}$ and $A_1^{(3)}$, respectively. In the bulk single crystal sample #14, we observed an additional mode at about 60 cm^{-1}, which we label as $A_1^{(1)}$. We associate these three features with vibration modes at the crystal surface, and will be discussed in the next section. We also noticed several sharp features below 50 cm^{-1} in sample #8 and #10 in RR, which are possibly zone folded phonons. To confirm this requires further studies, and is beyond the scope of this paper.

In the RL scattering geometry, we observed two weak features at 67 and 126 cm^{-1}, labeled $E^{(1)}$ and $E^{(2)}$, respectively (Fig. 1(b)). The energy of these modes are close to the strong bulk phonons, and therefore require higher resolution to distinguish them.

In Fig. 2 are the Raman spectra of the bulk sample at different excitation wavelengths at 10K. The spectra were obtained in the XX configuration. As in Fig. 1, we observe an additional peak at 158 cm−1 which we refer to as A_1^3. However, note the Fano line shape of the mode when 780 nm excitation wavelength is used. This is an indication that the $A_1^{(3)}$ phonon is interacting with a continuum.

Figure 3 shows the Raman spectra taken at 13 K with RR and RL scattering geometries on the bulk single crystal #14, where the smoother low resolution (2.8 cm^{-1}) is overlapped with the high resolution (0.9 cm^{-1}) spectra as guide to the eye. Besides the more pronounced $A_1^{(2)}$ and $A_1^{(3)}$ modes already visible in Fig. 1, we see a few additional features in the high resolution data: (1) A mode centered at 173 cm^{-1} appearing as a shoulder to the $A_{1g}^{(2)}$ bulk phonon in RR geometry (Fig. 3(a)), which we designate as $A_1^{(4)}$. (2) Another mode centered

at 126 cm^{-1} appearing as a shoulder to the $E_g^{(2)}$ bulk phonon in RL geometry (Fig. 3(b)), which we designate as $E^{(2)}$. (3) The mode $A_1^{(3)}$ shows double peak structure separated by about 3 cm^{-1}. This cannot be splitting due to lowering of symmetry since A_1 is a one-dimensional representation.

To further understand the origin of the observed phonon modes, we measure the Raman response in 4 scattering geometries of the D_{3d} and C_{3v} point group as listed in Table II (Fig. 4(a)). The intensity contributed by each symmetry channel in different scattering geometries are dictated by the Raman tensors [57, 58] and the results for D_{3d} and C_{3v} groups are listed in Table II. Therefore, by obtaining polarized Raman spectra in 4 proper scattering geometries, we can separate the measured Raman response from each symmetry channel.

$$\begin{aligned}\chi''_{A1g}(\omega)+\chi''_{A1}(\omega) &= \chi''_{XX}(\omega)-\frac{1}{2}\chi''_{RL}(\omega)\\ \chi''_{A2g}(\omega)+\chi''_{A2}(\omega) &= \chi''_{YX}(\omega)-\frac{1}{2}\chi''_{RL}(\omega)\\ \chi''_{Eg}(\omega)+\chi''_{E}(\omega) &= \frac{1}{2}\chi''_{RL}(\omega)\end{aligned} \tag{1}$$

The results are shown in Fig. 4(b). We notice that no lattice vibrational mode is observed in the A_{2g} and A_2 symmetry channels. This is expected since the Raman tensors for these two channels are antisymmetric, and commonly correspond to pseudo-vector-like excitations [58–60]. The featureless spectra containing justifies the validity of our symmetry analysis, and also help to simplify the interpretation of data obtained in RR geometry. Since the signal in A_{2g} and A_2 channels are negligibly small, we can claim that all vibration modes appearing in RR have either A_{1g} or A_1 symmetry, justifying our mode assignments in Fig. 1 and Fig. 3.

The $A_1^{(2)}$ mode happens to have energy very close to the $E_g^{(2)}$ phonon, making it particularly difficult for spectroscopic experiments to distinguish. Here, we utilize the symmetry properties to separately detect them with polarized light. The polarization leakage of optical elements are precisely measured and removed, and thereby excluding the possibility of $A_1^{(2)}$ being a trivial polarization leakage from the $E_g^{(2)}$ phonon.

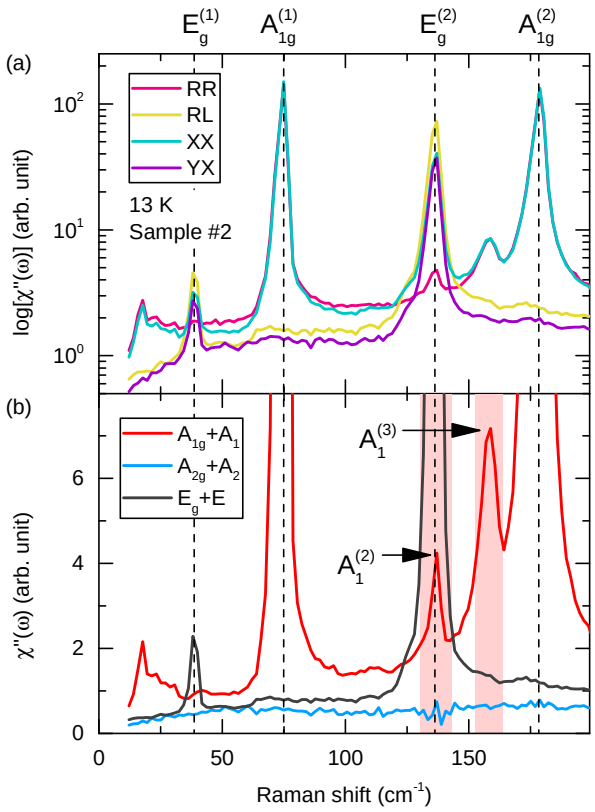

FIG. 4. (Color online) (a) The Raman spectra taken with all 4 scattering geometries at 13 K from a Bi_2Se_3 thin film, plot in semi-log scale. (b) The Raman response of different symmetry channels, obtained from data in (a). The bulk phonons are marked by dashed lines, whereas the surface modes are indicated by arrows and shaded in red.

IV. DISCUSSION

At the crystal surface of Bi_2Se_3, the lattice structure is distorted along c-axis due to the abrupt reduction of the interlayer van der Waals force that binds the crystal together. The surface distortion was calculated by density functional theory (DFT) to be about 10% along c-axis, and depicted in Ref. 61. Additionally, the observation of two-dimensional electron gas formed on Bi_2Se_3 surface is consistent with the subsurface van der Waals gap expansion [6, 63, 64]. As the lattice is distorted, the frequencies of atomic vibration modes at the surface are usually modified to a smaller value than in the bulk at the Brillouin zone center (Γ point) [25]. If there is a gap in the phonon density-of-state (DOS) and with large enough distortion, the surface phonon DOS can be entirely separated from the bulk [22, 25]. Such modes are long lived and localized at the surface, where the dispersion can be quite different than the bulk.

In Bi_2Se_3, there are some residual phonon DOS in the entire energy range [53], and the surface modes can decay into bulk phonon modes. If the frequency shift is small, where the DOS of the surface mode is not entirely separated from the bulk, then strictly speaking a localized surface mode does not exist. Instead, one would only expect a "surface resonance", which is only distinguishable from the bulk phonon by the slightly lower energy.

Due to inversion symmetry breaking at the crystal interface, the surface resonance from the Raman active A_{1g} and IR active A_{2u} phonons are both expected to appear in the A_1 symmetry (C_{3v} group), corresponding to out-of-plane atomic motion. This is consistent with the 4 A_1 modes we observed (Fig. 3(a)). From the energies

TABLE III. Summary of the phonon mode energies of Bi_2Se_3 measured in the current Raman scattering experiment, and previous studies reported in Ref. 35, 36, 47, and 61. Calculated results from two references [53, 62] are also listed for comparison. All values are given in units of cm^{-1}.

	Experiment		Calculation	
Symmetry	This work	Literature	LDA+SOI [53]	GGA+SOI [62]
$A_{1g}^{(1)}$	75	73 [36]	77	64
$A_{1g}^{(2)}$	180	175 [36]	176	167
$E_g^{(1)}$	39	39 [36]	41	39
$E_g^{(2)}$	137	133 [36]	139	124
$A_{2u}^{(1)}$	–	N/A	139	137
$A_{2u}^{(2)}$	–	N/A	161	156
$E_u^{(1)}$	–	61 [47]	80	65
$E_u^{(2)}$	–	133 [47]	131	127
$A_1^{(1)}$	60	68 [61]	N/A	N/A
$A_1^{(2)}$	136	129 [36]	N/A	N/A
$A_1^{(3)}$	158	160 [35, 36]	N/A	N/A
$A_1^{(4)}$	173	N/A	N/A	N/A
$E^{(1)}$	67	68 [36]	N/A	N/A
$E^{(2)}$	126	125 [36]	N/A	N/A

of these A_1 modes, we conclude that $A_1^{(1)}$ and $A_1^{(4)}$ are associated with the bulk phonon modes $A_{1g}^{(1)}$ and $A_{1g}^{(2)}$, respectively. The measured energy of the $A_1^{(1)}$ mode is somewhat different than the previously reported value of 68 cm^{-1} by time resolved ARPES in Ref. 61. This may be partly due to surface quality variation. ARPES measured sample is usually cleaved in ultra high vacuum, whereas the surface in this study is cleaved in nitrogen environment. This may also explain why this mode was never observed in the thin film samples (Fig. 1), where the sample is unavoidably exposed to air for a few minutes during the transfer between MBE chamber and Raman cryostat. The $A_1^{(4)}$ mode appears as a shoulder to the $A_{1g}^{(2)}$ bulk phonon, requiring higher resolution to distinguish from the bulk mode, and therefore was overlooked in the previous Raman study [36].

In comparison, the surface modes $A_1^{(2)}$ and $A_1^{(3)}$ have higher intensity and are better resolved. One possibility for this difference is that the bulk counterpart of these modes are the IR active $A_{2u}^{(1)}$ and $A_{2u}^{(2)}$ phonons, as the measured energy is close to the calculated values (Table III). Since these bulk modes are Raman inactive, we were able to better resolve the surface resonance. Another possibility is that the phonon DOS is practically zero at these energies in the A_1 symmetry channel, and the surface vibration modes are truly localized. Distinguishing these two scenarios is in fact experimentally non-trivial, especially since the experimental values of the $A_{2u}^{(1)}$ and $A_{2u}^{(2)}$ bulk phonon energies are yet unknown.

Nevertheless, both possibilities point to the surface origin of these two modes, which may provide us with information on the electron-phonon coupling at the TI surface. In particular, the double peak line shape of the $A_1^{(3)}$ phonon mode was overlooked in previous Raman studies and may be related to the 20 meV "kink" in the topological surface state's energy dispersion curve reported by ARPES measurements [33, 34].

On the other hand, while the bulk phonons show little resonance effect, the $A_1^{(3)}$ phonon displays antisymmetric line shape with near-infrared excitation (Fig. 2, inset). This suggests that there are surface electronic DOS that appear under resonance excitation with near-infrared wavelength [65, 66], which interacts with the $A_1^{(3)}$ phonon and results in the observed Fano line shape [67].

Since the in-plane symmetries are mainly preserved as the DFT calculated atomic surface distortion is purely out-of-plane [61], one would not expect any surface phonon with E symmetry (C_{3v} group) for Bi_2Se_3. However, the in-plane bonding potential is also modified by having distortion along c-axis, and therefore the phonon frequency at surface is still slightly different than the bulk value. If the modification is tiny, the E modes are expected to be weak and close to the bulk phonons. In Fig. 1(b) and Fig. 3(b), we can see hints of two additional modes, labeled by $E^{(1)}$ and $E^{(2)}$. The energies of these modes are in fact close to the measured values of $E_u^{(1)}$ and $E_u^{(2)}$ bulk phonons [45, 47], and are consistent with the previous Raman study [36] (Table III). However, the frequency of E_1 is slightly higher than $E_u^{(1)}$, which is against the expectation from a surface resonance. This may reflect the fact that this is an in-plane mode, orthogonal to the lattice distortion direction. Or, this may be indicative of non-trivial electron-phonon interaction with

the surface states, and worth further studying.

V. CONCLUSION

In conclusion, we have done a systematic symmetry analysis on the Raman spectra from high quality, freshly cleaved or grown *ab* surfaces of Bi_2Se_3 single crystal and thin films. We observed 4 out-of-plane and possibly 2 in-plane surface vibrational modes. The much larger intensity for the out-of-plane vibration modes is consistent with *c*-axis lattice distortion and van der Waals gap expansion calculated for Bi_2Se_3 crystal surface [61, 64]. The energies of the $A_1^{(1)}$ and $A_1^{(4)}$ modes are close to the bulk A_{1g} phonons. Due to the smallness of calculated crystal surface distortion [61] and the lack of phonon DOS gap [53], these modes are likely not fully localized or separated from bulk phonon DOS. However, the $A_1^{(2)}$ and $A_1^{(3)}$ modes are much stronger and sharper compared to the other vibration modes, and may be candidates of localized surface phonons. In particular, we found an anomalous double peak and Fano lineshape for the $A_1^{(3)}$ mode, both in low doped Bi_2Se_3 single crystals. The Fano lineshape is usually indicative of electron-phonon coupling, important for understanding the relaxation and scattering of surface state excitations. Here, we found that the Fano lineshape is dependent of the excitation energy, which may be able to explain the inconsistent surface electron-phonon coupling constant found in previous ARPES studies [19, 31].

ACKNOWLEDGMENTS

G.B. and H.-H.K acknowledge support from NSF Award DMR-1104884. H.-H.K. also acknowledges partial support from the U.S. DOE, BES grant DE-SC0005463. S.O., M.S., N.K. and M.B. are funded by Gordon and Betty Moore Foundation's EPiQS initiative (GBMF4418) and NSF(EFMA-1542798). S.-W.C. and X.W. acknowledge support from NSF Award DMREF-1233349.

[1] Liang Fu, C. L. Kane, and E. J. Mele, "Topological insulators in three dimensions," Phys. Rev. Lett. **98**, 106803 (2007).
[2] Haijun Zhang, Chao-Xing Liu, Xiao-Liang Qi, Xi Dai, Zhong Fang, and Shou-Cheng Zhang, "Topological insulators in Bi_2Se_3, Bi_2Te_3 and Sb_2Te_3 with a single Dirac cone on the surface," Nat. Phys. **5**, 438 (2009).
[3] D. Hsieh, Y. Xia, D. Qian, L. Wray, J. H. Dil, F. Meier, J. Osterwalder, L. Patthey, J. G. Checkelsky, N. P. Ong, A. V. Fedorov, H. Lin, A. Bansil, D. Grauer, Y. S. Hor, R. J. Cava, and M. Z. Hasan, "A tunable topological insulator in the spin helical Dirac transport regime," Nature **460**, 1101–1105 (2009).
[4] Y. Xia, D. Qian, D. Hsieh, L. Wray, A. Pal, H. Lin, A. Bansil, D. Grauer, Y. S. Hor, R. J. Cava, and M. Z. Hasan, "Observation of a large-gap topological-insulator class with a single Dirac cone on the surface," Nat. Phys. **5**, 398–402 (2009).
[5] J. G. Checkelsky, Y. S. Hor, M.-H. Liu, D.-X. Qu, R. J. Cava, and N. P. Ong, "Quantum interference in macroscopic crystals of nonmetallic Bi_2Se_3," Phys. Rev. Lett. **103**, 246601 (2009).
[6] Marco Bianchi, Dandan Guan, Shining Bao, Jianli Mi, Bo Brummerstedt Iversen, Philip D. C. King, and Philip Hofmann, "Coexistence of the topological state and a two-dimensional electron gas on the surface of Bi_2Se_3," Nat. Commun. **1**, 128 (2010).
[7] Haim Beidenkopf, Pedram Roushan, Jungpil Seo, Lindsay Gorman, Ilya Drozdov, Yew San Hor, R. J. Cava, and Ali Yazdani, "Spatial fluctuations of helical Dirac fermions on the surface of topological insulators," Nat. Phys. **7**, 939–943 (2011).
[8] M. Zahid Hasan and Joel E. Moore, "Three-dimensional topological insulators," Annual Review of Condensed Matter Physics **2**, 55–78 (2011).
[9] Liang Fu and C. L. Kane, "Superconducting proximity effect and majorana fermions at the surface of a topological insulator," Phys. Rev. Lett. **100**, 096407 (2008).
[10] Xiao-Liang Qi, Taylor L. Hughes, and Shou-Cheng Zhang, "Topological field theory of time-reversal invariant insulators," Phys. Rev. B **78**, 195424 (2008).
[11] Xiao-Liang Qi, Rundong Li, Jiadong Zang, and Shou-Cheng Zhang, "Inducing a magnetic monopole with topological surface states," Science **323**, 1184–1187 (2009).
[12] M. Z. Hasan and C. L. Kane, "*Colloquium* : Topological insulators," Rev. Mod. Phys. **82**, 3045–3067 (2010).
[13] Rui Yu, Wei Zhang, Hai-Jun Zhang, Shou-Cheng Zhang, Xi Dai, and Zhong Fang, "Quantized anomalous hall effect in magnetic topological insulators," Science **329**, 61–64 (2010).
[14] S. Raghu, Suk Bum Chung, Xiao-Liang Qi, and Shou-Cheng Zhang, "Collective modes of a helical liquid," Phys. Rev. Lett. **104**, 116401 (2010).
[15] Xiao-Liang Qi and Shou-Cheng Zhang, "Topological insulators and superconductors," Rev. Mod. Phys. **83**, 1057–1110 (2011).
[16] Y. H. Wang, H. Steinberg, P. Jarillo-Herrero, and N. Gedik, "Observation of Floquet-Bloch states on the surface of a topological insulator," Science **342**, 453–457 (2013).
[17] Tarun Grover, D. N. Sheng, and Ashvin Vishwanath, "Emergent space-time supersymmetry at the boundary of a topological phase," Science **344**, 280–283 (2014).
[18] N. P. Butch, K. Kirshenbaum, P. Syers, A. B. Sushkov, G. S. Jenkins, H. D. Drew, and J. Paglione, "Strong surface scattering in ultrahigh-mobility Bi_2Se_3 topological insulator crystals," Phys. Rev. B **81**, 241301 (2010).
[19] Z.-H. Pan, A. V. Fedorov, D. Gardner, Y. S. Lee, S. Chu, and T. Valla, "Measurement of an exceptionally weak electron-phonon coupling on the surface of the topolog-

ical insulator Bi_2Se_3 using angle-resolved photoemission spectroscopy," Phys. Rev. Lett. **108**, 187001 (2012).
[20] T. Valla, Z.-H. Pan, D. Gardner, Y. S. Lee, and S. Chu, "Photoemission spectroscopy of magnetic and nonmagnetic impurities on the surface of the Bi_2Se_3 topological insulator," Phys. Rev. Lett. **108**, 117601 (2012).
[21] V. Parente, A. Tagliacozzo, F. von Oppen, and F. Guinea, "Electron-phonon interaction on the surface of a three-dimensional topological insulator," Phys. Rev. B **88**, 075432 (2013).
[22] I. M. Lifshitz and L. N. Rosenzweig, "Dynamics of lattice filling half-space (Russian)," Zh. Eksp. Teor. Fiz. **18**, 1012 (1948).
[23] I. M. Lifshitz, "Some problems of the dynamic theory of non-ideal crystal lattices," Il Nuovo Cimento **3**, 716–734 (1956).
[24] Richard F. Wallis, "Effect of free ends on the vibration frequencies of one-dimensional lattices," Phys. Rev. **105**, 540–545 (1957).
[25] Richard F. Wallis, "Theory of surface modes of vibration in two- and three-dimensional crystal lattices," Phys. Rev. **116**, 302–308 (1959).
[26] G. Benedek and L. Miglio, "The green's function method in the surface lattice dynamics of ionic crystals," in *Surface Phonons*, edited by Winfried Kress and Frederik W. de Wette (Springer Berlin Heidelberg, Berlin, Heidelberg, 1991) pp. 37–66.
[27] R.F Wallis, "Surface phonons: theoretical developments," Surface Science **299**, 612 – 627 (1994).
[28] Xuetao Zhu, L. Santos, R. Sankar, S. Chikara, C. . Howard, F. C. Chou, C. Chamon, and M. El-Batanouny, "Interaction of phonons and Dirac fermions on the surface of Bi_2Se_3: A strong Kohn anomaly," Phys. Rev. Lett. **107**, 186102 (2011).
[29] Xuetao Zhu, L. Santos, C. Howard, R. Sankar, F. C. Chou, C. Chamon, and M. El-Batanouny, "Electron-phonon coupling on the surface of the topological insulator Bi_2Se_3 determined from surface-phonon dispersion measurements," Phys. Rev. Lett. **108**, 185501 (2012).
[30] C. Howard, M. El-Batanouny, R. Sankar, and F. C. Chou, "Anomalous behavior in the phonon dispersion of the (001) surface of Bi_2Te_3 determined from helium atom-surface scattering measurements," Phys. Rev. B **88**, 035402 (2013).
[31] Richard C. Hatch, Marco Bianchi, Dandan Guan, Shining Bao, Jianli Mi, Bo Brummerstedt Iversen, Louis Nilsson, Liv Hornekær, and Philip Hofmann, "Stability of the Bi_2Se_3(111) topological state: Electron-phonon and electron-defect scattering," Phys. Rev. B **83**, 241303 (2011).
[32] Z.-H. Pan, A. V. Fedorov, D. Gardner, Y. S. Lee, S. Chu, and T. Valla, "Measurement of an exceptionally weak electron-phonon coupling on the surface of the topological insulator Bi_2Se_3 using angle-resolved photoemission spectroscopy," Phys. Rev. Lett. **108**, 187001 (2012).
[33] Chaoyu Chen, Zhuojin Xie, Ya Feng, Hemian Yi, Aiji Liang, Shaolong He, Daixiang Mou, Junfeng He, Yingying Peng, Xu Liu, Yan Liu, Lin Zhao, Guodong Liu, Xiaoli Dong, Jun Zhang, Li Yu, Xiaoyang Wang, Qinjun Peng, Zhimin Wang, Shenjin Zhang, Feng Yang, Chuangtian Chen, Zuyan Xu, and X. J. Zhou, "Tunable Dirac fermion dynamics in topological insulators," Scientific Reports **3**, 2411 (2013).
[34] Takeshi Kondo, Y. Nakashima, Y. Ota, Y. Ishida, W. Malaeb, K. Okazaki, S. Shin, M. Kriener, Satoshi Sasaki, Kouji Segawa, and Yoichi Ando, "Anomalous dressing of Dirac fermions in the topological surface state of Bi_2Se_3, Bi_2Te_3, and Cu-doped Bi_2Se_3," Phys. Rev. Lett. **110**, 217601 (2013).
[35] A. Kogar, S. Vig, A. Thaler, M. H. Wong, Y. Xiao, D. Reig-i-Plessis, G. Y. Cho, T. Valla, Z. Pan, J. Schneeloch, R. Zhong, G. D. Gu, T. L. Hughes, G. J. MacDougall, T.-C. Chiang, and P. Abbamonte, "Surface collective modes in the topological insulators Bi_2Se_3 and $Bi_{0.5}Sb_{1.5}Te_{3-x}Se_x$," Phys. Rev. Lett. **115**, 257402 (2015).
[36] V. Gnezdilov, Yu. G. Pashkevich, H. Berger, E. Pomjakushina, K. Conder, and P. Lemmens, "Helical fluctuations in the raman response of the topological insulator Bi_2Se_3," Phys. Rev. B **84**, 195118 (2011).
[37] Mahmoud Eddrief, Paola Atkinson, Victor Etgens, and Bernard Jusserand, "Low-temperature Raman fingerprints for few-quintuple layer topological insulator Bi_2Se_3 films epitaxied on GaAs," Nanotechnology **25**, 245701 (2014).
[38] S. Y. F. Zhao, C. Beekman, L. J. Sandilands, J. E. J. Bashucky, D. Kwok, N. Lee, A. D. LaForge, S. W. Cheong, and K. S. Burch, "Fabrication and characterization of topological insulator Bi_2Se_3 nanocrystals," Applied Physics Letters **98**, 141911 (2011).
[39] Norbert Esser and Wolfgang Richter, "Raman scattering from surface phonons," in *Light scattering in solids VIII*, edited by Manuel Cardona and Gernot Güntherodt (Springer-Verlag, Berlin, 1999) pp. 96–168.
[40] Matthew Brahlek, Namrata Bansal, Nikesh Koirala, Su-Yang Xu, Madhab Neupane, Chang Liu, M. Zahid Hasan, and Seongshik Oh, "Topological-metal to band-insulator transition in $(Bi_{1-x}In_x)_2Se_3$ thin films," Phys. Rev. Lett. **109**, 186403 (2012).
[41] Namrata Bansal, Yong Seung Kim, Matthew Brahlek, Eliav Edrey, and Seongshik Oh, "Thickness-independent transport channels in topological insulator Bi_2Se_3 thin films," Phys. Rev. Lett. **109**, 116804 (2012).
[42] M. Emziane, S. Marsillac, and J.C. Bernde, "Preparation of highly oriented α-In_2Se_3 thin films by a simple technique," Materials Chemistry and Physics **62**, 84 – 87 (2000).
[43] McIver J. W., D. Hsieh, H. Steinberg, P. Jarillo-Herrero, and N. Gedik, "Control over topological insulator photocurrents with light polarization," Nat. Nanotechnol. **7**, 96–100 (2012).
[44] H. Khler and C. R. Becker, "Optically active lattice vibrations in Bi_2Se_3," physica status solidi (b) **61**, 533–537 (1974).
[45] W. Richter and C. R. Becker, "A Raman and far-infrared investigation of phonons in the rhombohedral V_2VI_3 compounds Bi_2Te_3, Bi_2Se_3, Sb_2Te_3 and $Bi_2(Te_{1-x}Se_x)_3$ $(0 < x < 1)$, $(Bi_{1-y}Sb_y)_2Te_3$ $(0 < y < 1)$," physica status solidi (b) **84**, 619–628 (1977).
[46] Jun Zhang, Zeping Peng, Ajay Soni, Yanyuan Zhao, Yi Xiong, Bo Peng, Jianbo Wang, Mildred S. Dresselhaus, and Qihua Xiong, "Raman spectroscopy of few-quintuple layer topological insulator Bi_2Se_3 nanoplatelets," Nano Letters **11**, 2407–2414 (2011).
[47] A. D. LaForge, A. Frenzel, B. C. Pursley, Tao Lin, Xinfei Liu, Jing Shi, and D. N. Basov, "Optical characterization of Bi_2Se_3 in a magnetic field: Infrared evidence for

magnetoelectric coupling in a topological insulator material," Phys. Rev. B **81**, 125120 (2010).
[48] T. Terzibaschian and B. Enderlein, "The irreducible representations of the two-dimensional space groups of crystal surfaces. theory and applications," physica status solidi (b) **133**, 443–461 (1986).
[49] Jian Li, Jiufeng J. Tu, and Joseph L. Birman, "Symmetry predicted transitions in 3D topological insulators," Solid State Communications **163**, 11 – 14 (2013).
[50] Robert-Jan Slager, Andrej Mesaros, Vladimir Juricic, and Jan Zaanen, "The space group classification of topological band-insulators," Nat. Phys. **9**, 98–102 (2013).
[51] R. Lewandowska, R. Bacewicz, J. Filipowicz, and W. Paszkowicz, "Raman scattering in α-In_2Se_3 crystals," Materials Research Bulletin **36**, 2577 – 2583 (2001).
[52] G.F. Koster, *Properties of the thirty-two point groups*, Massachusetts institute of technology press research monograph (M.I.T. Press, 1963).
[53] Bao-Tian Wang and Ping Zhang, "Phonon spectrum and bonding properties of Bi_2Se_3: Role of strong spin-orbit interaction," Applied Physics Letters **100**, 082109 (2012).
[54] Yuri D Glinka, Sercan Babakiray, Trent A Johnson, and David Lederman, "Thickness tunable quantum interference between surface phonon and Dirac plasmon states in thin films of the topological insulator Bi_2Se_3," Journal of Physics: Condensed Matter **27**, 052203 (2015).
[55] Liang Wu, M. Brahlek, R. Valdes Aguilar, A. V. Stier, C. M. Morris, Y. Lubashevsky, L. S. Bilbro, N. Bansal, S. Oh, and N. P. Armitage, "A sudden collapse in the transport lifetime across the topological phase transition in $(Bi_{1-x}In_x)_2Se_3$," Nat. Phys. **9**, 410–414 (2013).
[56] Hang Dong Lee, Can Xu, Samir M. Shubeita, Matthew Brahlek, Nikesh Koirala, Seongshik Oh, and Torgny Gustafsson, "Indium and bismuth interdiffusion and its influence on the mobility in In_2Se_3/Bi_2Se_3," Thin Solid Films **556**, 322 – 324 (2014).
[57] Manuel Cardona, "Resonance phenomena," in *Light scattering in solids II*, edited by Manuel Cardona and Gernot Güntherodt (Springer-Verlag, Berlin, 1982) pp. 45–49.
[58] L. N. Ovander, "The form of the Raman tensor," Opt. Spectrosc. **9**, 302 (1960).
[59] B. S. Shastry and B. I. Shraiman, "Raman Scattering in Mott-Hubbard Systems," Int. J. Mod. Phys. B **5**, 365–388 (1991).
[60] D. V. Khveshchenko and P. B. Wiegmann, "Raman scattering and anomalous current algebra in mott insulators," Phys. Rev. Lett. **73**, 500–503 (1994).
[61] J. A. Sobota, S.-L. Yang, D. Leuenberger, A. F. Kemper, J. G. Analytis, I. R. Fisher, P. S. Kirchmann, T. P. Devereaux, and Z.-X. Shen, "Distinguishing bulk and surface electron-phonon coupling in the topological insulator Bi_2Se_3 using time-resolved photoemission spectroscopy," Phys. Rev. Lett. **113**, 157401 (2014).
[62] Wei Cheng and Shang-Fen Ren, "Phonons of single quintuple Bi_2Te_3 and Bi_2Se_3 films and bulk materials," Phys. Rev. B **83**, 094301 (2011).
[63] Marco Bianchi, Richard C Hatch, Dandan Guan, Tilo Planke, Jianli Mi, Bo Brummerstedt Iversen, and Philip Hofmann, "The electronic structure of clean and adsorbate-covered Bi_2Se_3 : an angle-resolved photoemission study," Semiconductor Science and Technology **27**, 124001 (2012).
[64] T. V. Menshchikova, S. V. Eremeev, and E. V. Chulkov, "On the origin of two-dimensional electron gas states at the surface of topological insulators," JETP Letters **94** (2011).
[65] J. A. Sobota, S.-L. Yang, A. F. Kemper, J. J. Lee, F. T. Schmitt, W. Li, R. G. Moore, J. G. Analytis, I. R. Fisher, P. S. Kirchmann, T. P. Devereaux, and Z.-X. Shen, "Direct optical coupling to an unoccupied Dirac surface state in the topological insulator Bi_2Se_3," Phys. Rev. Lett. **111**, 136802 (2013).
[66] M. C. Wang, S. Qiao, Z. Jiang, S. N. Luo, and J. Qi, "Unraveling photoinduced spin dynamics in the topological insulator Bi_2Se_3," Phys. Rev. Lett. **116**, 036601 (2016).
[67] M.V. Klein, "Electronic raman scattering," in *Light Scattering in Solids I*, edited by M. Cardona and G. Güntherodt (Springer-Verlag, Berlin, 1983) pp. 169–172.